# Peripheral nerve graft architecture affects regeneration

Vleggeert-Lankamp, Carmen Lia Anne-Marie

CHAPTER 3

# Electrophysiology and morphometry of the Aα- and Aβ-fibre populations in the normal and regenerating rat sciatic nerve

C.L.A.M. Vleggeert-Lankamp[a], R.J. van den Berg[b], H.K.P. Feirabend[a], E.A.J.F. Lakke[a], M.J.A. Malessy[a], R.T.W.M. Thomeer[a]

[a]Neuroregulation group, Department of Neurosurgery, [b]Department of Neurophysiology, Leiden University Medical Centre (LUMC), P.O. Box 9600, NL-2300 RC Leiden, the Netherlands

*Exp Neurol, 2004; 187: 337-349*

*Ik verkondig de mening dat als het uiterlijk geslaagd is, het niet voor de hand ligt dat de hersenen mislukt zijn (Hans Dorrestijn gelooft niet in 'domme blondjes')*

## Abstract

We studied electrophysiological and morphological properties of the Aα- and Aβ-fibres in the regenerating sciatic nerve, to establish whether these fibre types regenerate in numerical proportion, and whether and how the electrophysiological properties of these fibre types are adjusted during regeneration.

Compound action potentials were evoked from isolated sciatic nerves twelve weeks after autografting. Nerve fibres were gradually recruited either by increasing the stimulus voltage from subthreshold to supramaximal levels, or by increasing the interval between two supra-maximal stimuli, in order to obtain the cumulative distribution of the extracellular firing thresholds and refractory periods respectively. Thus the mean conduction velocity, the maximal charge displaced during the compound action potential ($Q_{max}$), the mean firing threshold ($V_{50}$) and the mean refractory period ($t_{50}$) were determined. The number of myelinated nerve fibres and their fibre diameter frequency distributions were determined in the peroneal nerve.

Mathematical modelling applied to fibre recruitment- and diameter distributions allowed discrimination of the Aα- and Aβ-fibre populations. In regenerating nerves the number of Aα-fibres increased fourfold, while the number of Aβ-fibres did not change. In regenerating Aα- and Aβ-fibres the fibre diameter decreased and $V_{50}$ and $t_{50}$ increased. The regenerating Aα-fibres' contribution to $Q_{max}$ decreased considerably, while that of the Aβ-fibres remained the same. Correlation of the electrophysiological data to the morphological data provided indications that the ion channel composition of both the Aα- and the Aβ-fibres are altered during regeneration. This demonstrates that combining morphometric and electrophysiological analysis provides better insight in the changes that occur during regeneration.

## Introduction

The evaluation of the efficacy of the experimental repair of peripheral nerve lesions often focuses on the presence of regenerating nerve fibres in the distal nerve stump. The number of regenerated nerve fibres, whether or not combined with the nerve fibre diameter, is generally considered to be the decisive factor for the success of nerve repair. Although it is generally presumed that regenerating nerve fibres are able to conduct an action potential, research in this area is only performed parsimoniously. Though it is well known that during regeneration the mean conduction velocity decreases, little is known about other electrophysiological parameters like firing threshold and refractory period in general [17, 47], and nothing is known about these parameters with respect to the Aα- and the Aβ-fibres. Studies that relate morphological to electrophysiological data are likewise scarce [4, 8, 17, 28].



In regenerating rat sciatic nerves, the number of nerve fibres either increases [3, 9, 20, 21, 50, 53], or remains the same [12, 28, 32], while the average diameter decreases [3, 9, 12, 20, 21, 28, 32, 50, 53]. The increase in the number of fibres is generally attributed to branching, but it is not known whether Aα- and Aβ-fibres regenerate and branch proportionally. Previous studies in control nerves demonstrate that the diameter of nerve fibres is inversely related to the firing threshold [6, 17, 18] and to the refractory period [6, 37]. As the diameter decreases during nerve regeneration, changes of firing threshold and refractory period are to be expected. In the present study, we specifically aimed to establish whether the number of Aα-fibres (comprising both the α-motoneuronal axons ánd the Ia/b sensory afferent axons) in the regenerating nerve increased in proportion to the number of Aβ-fibres, and whether and how the electrophysiological properties of these fibre types are altered during regeneration.

We investigated changes in the composition of the regenerating nerve with respect to its constituent fibre types, both electrophysiologically and morphologically. The extracellular firing threshold, refractory period, and charge displacement during a compound action potential in the rat sciatic nerve were related to the number and diameter of nerve fibres, both in control and autografted nerves. Mathematical models were applied to the electrophysiological and morphometrical data to separate the contribution of the Aα- and the Aβ-fibres.

## Materials and Methods

### *Animal model*

Female Wistar rats (HsdCpb:WU), weighing 220-240 grams and housed in flat bottomed cages in a central animal-care facility, were maintained on a 12-hour light cycle regime at a controlled temperature of 22°C. Standard rat chow and water were available *ad libitum*. Autograft experiments were performed on the left sciatic nerve. Unoperated rats served as controls. All experiments were performed in accordance with international and local laws governing the protection of animals used for experimental purposes (UDEC 99105).

*Autograft procedure*

For the grafting procedure, rats were given a general inhalation anaesthesia of isoflurane in a 1:1 mixture of $O_2$ and $N_2O$. To improve anaesthesia and to diminish post-operative pain, buprenorphine (0.1 ml of 0.3 mg/ml; Temgesic®, Schering-Plough, Maarssen, the Netherlands) was injected intra-peritoneally. All animals were operated in the same time span by the same surgeon. Under aseptic conditions the left sciatic nerve was exposed and isolated at the midthigh level via a dorsal approach, and a 6 mm nerve segment was resected. This nerve segment was reversed longitudinally and grafted into the gap with 4 epineurial sutures (10-0 monofilament nylon) at each end. The post-operative survival period was 12 weeks.

*Electrophysiological analysis*



To collect the control (n = 12) and autografted (n = 12) nerves, the rats were anaesthetized as described above. As long a segment as possible of the (autografted) sciatic nerve was resected and the animals were euthanized. The isolated (autografted) nerve was immersed in a standard solution (see below) on a cooled (4°C) glass plate and cleaned under a dissection microscope. The epineurium was carefully resected. In the autografted nerves, we choose to remove only 5 to 10 mm of epineurium from the proximal and distal ends, and to leave the graft, located entirely in the middle pool (see below), intact.

The nerve was mounted across the five pools of the five compartment moist chamber [48]. The pools were filled with standard solution composed of: 140 mM NaCl, 3.0 mM KCl, 1.5 mM $CaCl_2$, 1.25 mM $MgSO_4$, 11.0 mM glucose, and 5.0 mM Tris buffer (pH 7.4, 20 °C). The proximal nerve crossed pools 1 and 2 and the distal nerve pools 4 and 5 (fig. 1).

In order to measure monophasic action potentials, the nerve fibres in pool 1 (and 5) were made inexcitable by replacing $Na^+$ in the standard solution with choline $^+$. The nerve fibres were excited extra-cellularly with a voltage pulse of 100 µs. The propagated compound action potential was measured as the potential difference ($V_{1-2}$) between pools 1 and 2 (4 and 5 in orthodromic recording, see below), and normalized in terms of compound action currents [48].

Each compound action current is characterized by its maximum amplitude and duration. The duration of the action current was defined as the width of the action potential at 50% of the maximum amplitude. To take into account both the amplitude and the duration, the response was expressed as the *area under the action current* (Q), corresponding to the displaced electrical charge. The *maximal charge displaced* ($Q_{max}$) was defined as the area under the curve of the maximal action current (upon increase to the supra-maximal stimulus voltage), and the *mean voltage threshold* ($V_{50}$) as the stimulus voltage at 50% $Q_{max}$. The *mean conduction velocity* (MCV) was calculated as the ratio of the conducting distance and the latency time to the peak of the maximal action current. Rundown of the compound action current due to deterioration of the nerve fibres was calculated from the spontaneous changes of $Q_{max}$ during the measurement time, and amounted to 4%/hr in control nerves and 10%/hr in autografted nerves. The measurements never lasted more than one hour.

*Figure 1:* Moist chamber schematic.

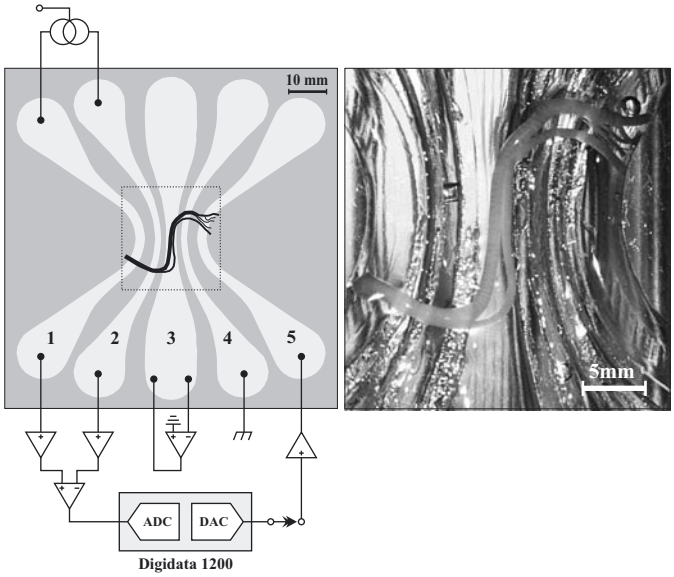


The diagram on the left depicts the five compartments of the moist chamber, drawn to scale. A nerve, crossing the five baths, is drawn to demonstrate its position. The pools are numbered 1 to 5. The proximal end of the sciatic nerve segment crosses pools 1 and 2, the grafted segment is entirely in pool 3 and the distal end of the sciatic nerve segment, which branches into the peritoneal and tibial nerves, crosses pools 4 and 5. The electrical circuit is configured for antidromic stimulation. The electrodes are represented by solid circles. The stimulus voltage is the output of a voltage-driven high-voltage amplifier, applied between pools 4 (cathode) and 5. The central pool, 3, is clamped at ground potential by a feedback amplifier. Electrodes connect pools 1 and 2 to the pre-amplifiers (triangles), which outputs are fed into a differential amplifier to measure the voltage difference between the two pools, and this signal is digitized by the ADC of the Digidata 1200 interface (Axon Instruments). With another pair of electrodes, a current from a voltage-driven current source (intertwined circles) can be injected through pools 1 and 2 to measure the magnitude of the resistance $R_{1\text{-}2}$. Both the current source and the high-voltage amplifier are driven by the DAC of the Digidata 1200. The adjacent photograph depicts a control nerve positioned over the pools of the moist chamber. Its 'S' shape is clearly visible and corresponds to that within the highlighted central section of the previous diagram.



The experimental set-up allowed for stimulation and measurement in two directions: orthodromic and antidromic. Previous experiments using the relatively thin sural nerve [48] yielded identical values for the action current conducted either ortho- or antidromically. Stimulation of the thick proximal end of the sciatic nerve (orthodromic) resulted in a large capacitive current artifact. In control nerves, the artifact partially overlapped with the action currents. In autografted nerves, where the action current appeared later, thus allowing better separation from the stimulus artifact, both directions of stimulation yielded comparable values for $Q_{max}$ ($p = 0.061$) and MCV ($p = 0.377$). The distal nerve stump of the sciatic nerve is branched into the peroneal and tibial nerve, resulting in a lower resistance between the recording pools, hence in a worse signal to noise ratio in orthodromic stimulation. We therefore choose to base our observations on the measurements of Q after antidromic stimulation, as did other authors using a similar experimental paradigm [22, 27, 41].

## Stimulus recruitment

To gain insight in the fibre type composition of the nerves, the constituent fibres were gradually recruited by increasing the stimulus voltage from sub-threshold to supra-maximal levels. The extra-cellular firing threshold of nerve fibres is inversely proportional to the fibre diameter [6, 25, 42]. Although the recruitment order will also be influenced by the geometrical spread of the Ranvier nodes, it was shown in rat nerves that the thicker nerve fibres are likely to be recruited before the thinner ones upon gradual increase of the stimulus [49].

To derive the contributions of the Aα- and Aβ-fibres to the compound action current we adopted the method of Van den Berg et al. [48]. The gradual recruitment of the Aα-fibres (comprising both the α-motoneuronal axons ánd the Ia/b sensory afferent axons) as a function of the stimulus voltage (stimulus-recruitment relation) is described by the cumulative normal distribution of the Aα threshold voltages



$$Q_{\alpha}(V) = \frac{1}{2} Q_{max,\alpha}\left(1 + erf\,\frac{(V - V_{50,\alpha})}{k_{\alpha}}\right) \quad (1)$$

where $Q_{\alpha}(V)$ is the integral of the Aα action current, and $Q_{max,\alpha}$ the value of $Q_{\alpha}(V)$ at supra-maximal stimulus. The parameter $V_{50,\alpha}$ (the mean firing threshold, or, more precisely, the *mean threshold voltage*) is the stimulus voltage at 50% $Q_{max,\alpha}$. The $k_{\alpha}$ reflects the slope of the recruitment curve at $V_{50,\alpha}$. The recruitment of the Aβ-fibres can be described by the same equation. An *erf* function is an 'error' function encountered in integrating a normal distribution [1].

At short conduction distances, when the Aα- and Aβ-action currents are overlapping, the contributions of Aα- and Aβ-fibres can be derived from the compound action current by fitting the sum of two cumulative normal distributions of voltage thresholds to the stimulus-recruitment curve [48]:

$$Q(V) = \frac{1}{2}\left[Q_{max,\alpha}\left(1 + erf\,\frac{(V - V_{50,\alpha})}{k_{\alpha}}\right) + Q_{max,\beta}\left(1 + erf\,\frac{(V - V_{50,\beta})}{k_{\beta}}\right)\right] \quad (2)$$

Q(V) is the integral of the compound action current. Fitting eq. 2 to the data recorded in the stimulus-recruitment experiments yielded the values of $Q_{max,\alpha}$, $Q_{max,\beta}$, $V_{50,\alpha}$, and $V_{50,\beta}$.

To evaluate the validity of fitting with eq. 2 instead of eq. 1 Akaike's Information Criterium (AIC) was used. The AIC adjudges a numerical value to the fit which is a measure for the quality of the fit. The lower the value, the better the fit. Moreover, residual values of the fittings were determined to illustrate the quality of the fit.

## Interpulse time recruitment

To study the refractory period, we applied a similar approach. Compound action currents were recorded at increasing time intervals between two identical supra-maximal voltage pulses (100 μs). At short intervals, most to all nerve fibres are refractory and will not fire in response to a second stimulus. However, when the time span between pulses (interpulse time) gradually increases, progressively more nerve fibres will have recovered from refractoriness, and

can contribute to the second action current. The *mean refractory period* ($t_{50}$) was defined as the stimulus interval at which the area under the curve of the second action current amounted to 50% of the area under the curve at the supra-maximal stimulus voltage.

The contribution of Aα- and Aβ-fibres could also be derived from the second compound action current in response to gradually increasing stimulus intervals. The refractory period of nerve fibres is inversely proportional to the conduction velocity, and thus to the fibre diameter [37]. Depending on the stimulus interval, the second action current will thus be composed of varying contributions of Aα- and Aβ-fibres. After the shorter stimulus intervals predominantly the thicker Aα-fibres will be excited, whereas after larger intervals both the Aα- and the Aβ-fibres will be excited. Thus, in analogy to stimulus-recruitment, the order of recruitment will be reflected in the interpulse time-recruitment relation. Contrary to stimulus-recruitment, the spread of the Ranvier nodes at the stimulation site does not play a role as only supra-maximal stimuli are applied.



Assuming there is a Gaussian distribution of the refractory periods of both the Aα- and Aβ-fibres [cf. 29], the relation between Q and the interpulse time Δt (interpulse time-recruitment relation) should be described by

$$Q(\Delta t) = \frac{1}{2}\left[ Q_{max,\alpha}\left(1 + erf\,\frac{(\Delta t - t_{50,\alpha})}{r_\alpha}\right) + Q_{max,\beta}\left(1 + erf\,\frac{(\Delta t - t_{50,\beta})}{r_\beta}\right)\right] \quad (3)$$

where Q(Δt) is the integral of the second action current evoked at interpulse time Δt. $Q_{max,\alpha}$ and $Q_{max,\beta}$ represent the values of $Q_\alpha$ and $Q_\beta$ when, respectively, all Aα- or Aβ-fibres are recruited at the maximum stimulus interval; and $t_{50,\alpha}$ and $t_{50,\beta}$ represent the *mean refractory periods*. The $r_\alpha$ and $r_\beta$ reflect the slope of the recruitment curve at $t_{50,\alpha}$ and $t_{50,\beta}$, respectively. Eq. 3 was fitted to the data recorded in the interpulse time-recruitment experiments, and the values of $Q_{max,\alpha}$, $Q_{max,\beta}$, $t_{50,\alpha}$, and $t_{50,\beta}$ were estimated. Our description with eq. 3 was compared with fittings with a function containing a single *erf*-function using the AIC.

### *Morphometrical analysis*

As the ratio of myelinated and unmyelinated fibres, and the ratio of myelinated motor and sensory fibres are almost equal in the sciatic, the tibial and the peroneal nerve [43], we elected to analyze the peroneal nerve only. Since upon regeneration across sciatic nerve gap lesions of less than 8 mm the ratio of myelinated and unmyelinated fibres remains the same in the sciatic nerve branches [26], the composition of the peroneal nerve will arguably remain representative for the composition of the sciatic nerve.

After the electrophysiological recordings, the sciatic nerve was stored in a 4% formaldehyde solution. Subsequently, 5 to 10 mm long peroneal nerve samples were dissected out for morphometric analysis. The immersion fixation was continued for some days in a modified Karnovsky fixative, containing 2% paraformaldehyde and 1.25% glutaraldehyde [14, 16]. The tissue samples were osmicated in 1% solution of osmium tetroxide for 2 hr under constant agitation. Before and after osmication, the tissue was repeatedly rinsed in 0.1 M phosphate

buffered saline at pH 7.2. After gradual dehydration in ethanol, the osmicated nerve samples were embedded in Epon® (Merck, Amsterdam, The Netherlands). Transverse 1 µm sections were cut on a Reichert ultramicrotome (Leica, Rijswijk, The Netherlands), and stained with a 1% toluidine blue / 1% borax solution [14]. In the autografted group, all peroneal nerves were evaluated (n = 12) while in the control group aselectly chosen peroneal nerves were analyzed (n = 4).

Microscopic video images covering 3 sample areas of approximately 21000 µm² each (i.e. 50-75% of the total area of the nerve) were taken at a magnification of 40x. All light microscopically identifiable myelinated fibres in the sample areas were counted (*number of fibres*), and their profile areas (*fibre areas*), as well as the total surface of the nerve (*nerve area*) were measured automatically using a Zeiss Kontron KS-400 image analyser (Carl Zeiss, Weesp, The Netherlands) at a magnification of 890x. The fibre area included the area of both the axon and the myelin sheath profile. The *fibre diameter* (calculated from the imaginary circle corresponding to the fibre area ($2\sqrt{(\text{fibre area}/\pi)}$)), the *mean fibre area* (sum of fibre areas per sample / number of nerve fibres per sample), the *fibre density* (number of nerve fibres per 1000 µm²), and the *relative area of interspace* ((sample area – the sum of fibre areas per sample) x 100%/ sample area) were calculated. The *total number of fibres* per nerve was estimated (nerve area x (number of nerve fibres per sample/ sample area)).



Diameters of the nerve fibres were distributed into 180 classes of 0.1 µm each, and plotted versus the percentage of the number of fibres present in that class. The frequency distribution of the fibre diameters may reflect the two fibre populations identified by our electrophysiologic recordings. Given the gaussian distribution of firing thresholds together with the inverse relation between threshold and fibre diameter, a skewed frequency distribution of diameters for a single population of nerve fibres can be expected. Therefore, a lognormal function is likely to describe the distribution of fibre diameters [13, 15]. To evaluate the possible contributions of the Aα- and Aβ-fibre populations, the sum of two lognormal functions was fitted to the fibre diameter size distributions:

$$F(d) = F_{max,\alpha}\, e^{-\frac{\ln^2(d/d_{Fmax,\alpha})}{2w_\alpha^2}} + F_{max,\beta}\, e^{-\frac{\ln^2(d/d_{Fmax,\beta})}{2w_\beta^2}} \qquad (4)$$

where F(d) is the fibre diameter class frequency, $d_{Fmax,\alpha}$ the fibre diameter most frequently present in the Aα-fibre population, $F_{max,\alpha}$ the fibre diameter class frequency at $d_{Fmax,\alpha}$, and $w_\alpha$ the exponent related to the spread in diameter of the Aα-fibre population. The description according to eq. 4 was compared to fittings with a single lognormal function using the AIC.

Finally, the area under the resulting fibre diameter frequency distribution curves for the Aα- and Aβ-fibre populations was calculated, to estimate the percentage and subsequently the number of nerve fibres in each population.

*Statistics*

The means of all parameters were calculated and shown with standard deviations (SD). Paired and unpaired Student's t-tests were applied to the means to compare parameters. Differences between AICs derived from fits using 2 functions and fits using 1 function were tested for significance using paired t-tests. Kolmogorov-Smirnow tests were applied to the different nerves and to the different samples per nerve for comparison of size distributions [30, 46]. The SPSS statistical program, version 10.0, and Origin, version 5.0, were used for statistical analysis. P-values of less than 0.050 were regarded as significant.

## Results



*Gross examination*

All autografted nerves exhibited a graft in continuity at 12 weeks after surgery. Each autografted nerve was examined macroscopically and displayed a slight attenuation in diameter of the grafted part. The proximal and distal nerves appeared firm and shiny white, and the distal stump did not display the softening one would expect after Wallerian degeneration [44]. Some connective tissue was present around the coaptation sites, nevertheless the autografted nerves could be resected easily.

*Electrophysiology*

Stimulus recruitment

Typical examples of the extra-cellular action currents measured in control and autografted nerves are represented in figures 2A and B. In response to increasing stimulus voltages, the amplitude of the monophasic action current gradually increased until a maximum amplitude was reached. Both control and autografted nerves displayed this behaviour. In autografted nerves the action currents started later and the latency to the peak action current was longer. As a result, MCV was about three times smaller in autografted nerves (table 1). The amplitude of the peak action current was smaller and the duration of the action current was longer in autografted nerves at supra-maximal stimulus. Nevertheless, the value of $Q_{max}$ was less than half the control value.

The corresponding stimulus-recruitment curves exhibited two limbs: a steeply rising limb at low levels of the stimulus voltage, reflecting the excitation of the Aα-fibres, and a less steeply rising limb at higher stimulus voltages, reflecting the excitation of the Aβ-fibres [48] (fig. 2C and D). The curves of the autografted nerves were conspicuously different from those of the control nerves: (i) there was a shift to the right, to higher stimulus voltages; (ii) the initial limb of the curve was less steep, and, as mentioned earlier; (iii) $Q_{max}$ was more than halved. The mean voltage threshold ($V_{50}$) was higher in autografted nerves.

*Figure 2.* Stimulus-recruitment relations.

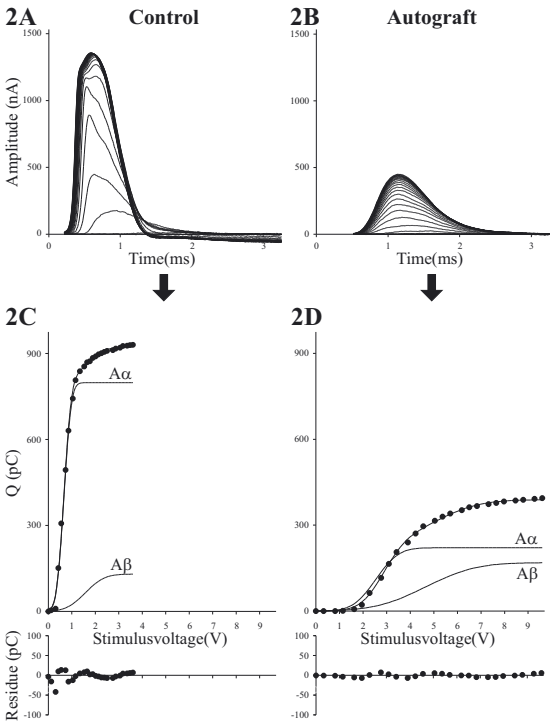


Typical examples of the time course of compound action currents as a function of stimulus voltage of both a control (fig. 2A) and an autografted nerve (fig. 2B). In each graph, the curves from bottom to top represent compound action currents, evoked by increasing stimulus voltages. Stimulus artifacts were erased. Due to the virtual cathode effect [31], upon increasing the voltage stimuli, the onset of the current moves closer to the stimulus artifact.
Figure 2C and D represent stimulus-recruitment graphs corresponding to the data given in figure 2A and B. Solid circles represent data points. Continuous lines represent the fitted curves. The separate curves of the Aα- and Aβ-fibres were calculated according to eq. 2. To illustrate the quality of the fit, small graphs below each main graph demonstrate the differences between measured and calculated data (residual values).

Fitting eq. 3 to the data demonstrated that in control nerves the contribution of the Aα-fibres to $Q_{max}$ ($Q_{max,\alpha}$) was larger than $Q_{max,\beta}$, and that the mean threshold voltage of the Aα-fibres ($V_{50,\alpha}$) was approximately half of $V_{50,\beta}$ (table 1).

In autografted nerves, the Aα-fibres' contribution to $Q_{max}$ ($Q_{max,\alpha}$) decreased notably, even becoming comparable to $Q_{max,\beta}$, while $Q_{max,\beta}$ did not decrease significantly (table 1). As in control nerves, $V_{50,\beta}$ was about two times higher than $V_{50,\alpha}$. However, both values more than doubled compared to control values.

Both in control and in autografted nerves, the AIC proved to be smaller ($p<10^{-4}$) for two populations compared to one, and the residual values were small (fig. 2C, bottom).

*Table 1.* Electrophysiological parameters

**Stimulus-recruitment**

| | | Control n = 12 | | | Autograft n = 12 | | | p | |
|---|---|---|---|---|---|---|---|---|---|
| **MCV** | m/s | 38.7 ± 9.0 | | | 12.5 ± 2.6 | | | $<10^{-4}$ | |
| $\mathbf{Q}_{max}$ | pC | 1007 ± 262 | | | 494 ± 195 | | | $<10^{-4}$ | |
| $\mathbf{V}_{50}$ | V | 0.8 ± 0.2 | | | 2.9 ± 1.0 | | | $<10^{-4}$ | |
| | | **α** | **β** | $\mathbf{p}_{\alpha\beta}$ | **α** | **β** | $\mathbf{p}_{\alpha\beta}$ | $\mathbf{p}_{\alpha\alpha}$ | $\mathbf{p}_{\beta\beta}$ |
| $\mathbf{Q}_{max,\alpha/\beta}$ | pC | 760 ± 310 | 247 ± 146 | 0.001 | 281 ± 100 | 213 ± 135 | 0.125 | $<10^{-4}$ | 0.571 |
| $\mathbf{V}_{50,\alpha/\beta}$ | V | 0.7 ± 0.1 | 1.4 ± 0.3 | $<10^{-4}$ | 1.9 ± 0.6 | 3.8 ± 1.1 | $<10^{-4}$ | $<10^{-4}$ | $<10^{-4}$ |

**Interpulse time-recruitment**

| | | Control n = 12 | | | Autograft n = 12 | | | p | |
|---|---|---|---|---|---|---|---|---|---|
| $\mathbf{Q}_{max}$ | pC | 832 ± 182 | | | 438 ± 162 | | | $<10^{-4}$ | |
| $\mathbf{t}_{50}$ | ms | 2.0 ± 0.3 | | | 4.9 ± 0.7 | | | $<10^{-4}$ | |
| | | **α** | **β** | $\mathbf{p}_{\alpha\beta}$ | **α** | **β** | $\mathbf{p}_{\alpha\beta}$ | $\mathbf{p}_{\alpha\alpha}$ | $\mathbf{p}_{\beta\beta}$ |
| $\mathbf{Q}_{max,\alpha/\beta}$ | pC | 640 ± 177 | 193 ± 65 | $<10^{-4}$ | 292 ± 116 | 146 ± 59 | 0.001 | $<10^{-4}$ | 0.093 |
| $\mathbf{t}_{50,\alpha/\beta}$ | ms | 1.8 ± 0.3 | 4.0 ± 0.4 | $<10^{-4}$ | 2.3 ± 0.4 | 6.9 ± 1.2 | $<10^{-4}$ | 0.002 | $<10^{-4}$ |

Values are represented as mean ± SD. The significance of the differences between the values is represented as $p_{\alpha\beta}$, $p_{\alpha\alpha}$ and $p_{\beta\beta}$ ; the subscript indicates the fibre classes relevant to the comparison. Unpaired Student's t-tests were applied to obtain $p_{\alpha\alpha}$- and $p_{\beta\beta}$-values and paired Student's t-tests were applied to obtain $p_{\alpha\beta}$-values.



## Interpulse time recruitment

Figures 3A and B represent the measured action currents as a function of the interval between two supra-maximal voltage stimuli in the same control and autografted nerves as represented in figure 2. At increasing interpulse times, the amplitude of the second action current gradu - ally increased to a maximum, while its duration decreased. Nevertheless the area under the curve of the second action current increased progressively. Both control and autografted nerves displayed this behaviour.

In autografted nerves, initiation of recruitment occurred at a longer interpulse time. The value of $Q_{max}$ was half the value of $Q_{max}$ in control nerves, in accordance with the results ob - tained from the stimulus-recruitment curves (table 1).

Figures 3C and D demonstrate the corresponding interpulse time-recruitment curves for the control and autografted nerves. As did the stimulus-recruitment curves, the interpulse time-recruitment curves clearly exhibited two limbs: a steeply rising limb at short stimulus intervals, reflecting the excitation of the Aα-fibres, and a less steeply rising limb at longer stimulus intervals, reflecting the excitation of the Aβ-fibres. The interpulse time-recruitment curve of the autografted nerves was clearly different from the curve of the control nerves: (i) there was a shift to the right, to larger interpulse times; (ii) the initial limb of the curve was less steep, and, as stated earlier; (iii) $Q_{max}$ was halved. The response in the autografted nerves was characterized by a larger mean refractory period ($t_{50}$) compared to control nerves (table 1). Fitting eq. 3 to the data demonstrated that in control nerves $Q_{max,\alpha}$ was significantly larger than $Q_{max,\beta}$ (table 1), and that the mean refractory period of the Aα-fibres ($t_{50,\alpha}$) was less than half of

$t_{50,\beta}$. In autografted nerves, $Q_{max,\alpha}$ was notably decreased but still significantly larger than $Q_{max,\beta}$, while $Q_{max,\beta}$ remained the same (table 1). The mean refractory period of the regenerating Aβ-fibres ($t_{50,\beta}$) was three times higher than $t_{50,\alpha}$, as in control nerves. Moreover, both values were more than a factor 1.5 higher compared to control nerves.

Both in control and in autografted nerves, the AIC proved to be smaller ($p<10^{-4}$) for two populations compared to one, and the residual values were small (fig. 2C, bottom).

### *Morphometry*

Light microscopy of sections demonstrated that regenerating nerves were vascularized and enclosed in a connective-tissue sheath. They contained many myelinated axons, abundant



*Figure 3.* Interpulse time-recruitment relations.

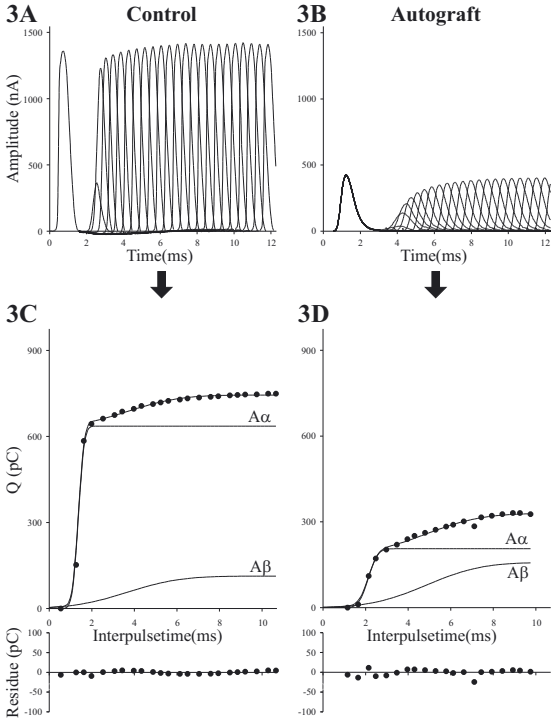


Typical examples of the time course of compound action currents, evoked by two consecutive supra-maximal voltage stimuli, with increasing interpulse times. The data were obtained from the same control and autografted nerves as represented in figure 2. In each graph, the leftmost curve represents the first action current and the following curves from left to right represent the action currents resulting from the second stimulus at increasing stimulus intervals. Stimulus artifacts were erased.

Figure 3C and D respresent interpulse time-recruitment graphs corresponding to the data given in figure 3A and B. Solid circles represent data points. Continuous lines represent the fitted curves. The separate curves of the Aα- and Aβ-fibres were calculated according to eq. 3. The theoretical dataset ($\Delta t = 0$, $Q = 0$) was added to the data. The quality of the fit is shown in the small graphs below each of the main graphs, which illustrates the negligible differences between our own measurements and the calculated data (residual values).

endoneurial collagen, and blood vessels. It is demonstrated in figure 4 that the area of the regenerating nerve (fig. 4C) was comparable to the area of the control nerve (fig. 4A). The nerve fibres in regenerating nerves (fig. 4D) were obviously more abundant in number, but much smaller in diameter compared to control nerves (fig. 4B). The myelin sheath of the nerve fibres was thinner in regenerating nerves. The morphometric analysis demonstrated that in regenerating nerves the number of nerve fibres was doubled, and that the fibre diameters were halved, while the areas of the control and autografted nerves were comparable (table 2). Therefore the fibre density and the relative interspace between the nerve fibres were larger in the regenerating nerve, while the fibre area was smaller. The Kolmogorov-Smirnow test revealed a homogeneous fibre size distribution throughout control nerves, and a homo - geneous fibre size distribution within individual control nerves. In the regenerating nerves both heterogeneity and homogeneity in fibre size distributions between nerves, and within individual nerves, were encountered.



Fitting eq. 4 to the fibre diameter frequency distributions demonstrated two maxima at approximately 4 and 9 µm in control nerves (fig. 5A), and at 2 and 3 µm in regenerating nerves (fig. 5B). In control nerves, the contribution of the Aβ-fibres to the total number of fibres was higher (60%) compared to the contribution of the Aα-fibres (40%). Additionally, the value of $d_{Fmax,\beta}$ was half the value of $d_{Fmax,\alpha}$. In regenerating nerves however, the Aβ-fibre population, was much smaller in number, about one fourth, compared to the Aα-fibre population. The

*Figure 4.* Light microscopic cross-sections of the peroneal nerve of control and autografted nerves.

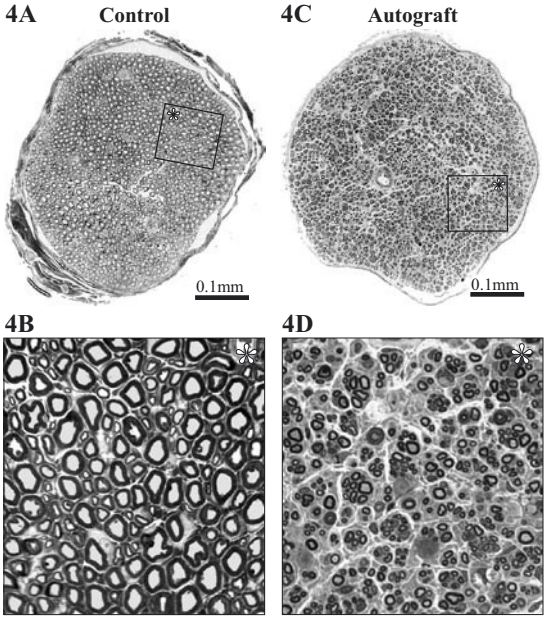


Transverse 1 µm sections of peroneal nerves were stained with toluidine blue. Figure 4A displays the entire cross-section of a control nerve, and figure 4B displays an enlarged sample of this nerve section (square), demonstrating the morphology of the nerve in detail. Accordingly, figure 4C displays a regenerating nerve and figure 4D shows this nerve in detail. The rotation of the samples is indicated with an asterix in the corner.

*Table 2.* Nerve morphometrical parameters

| | | Control n = 4 | | | Autograft n = 12 | | | | | |
|---|---|---|---|---|---|---|---|---|---|---|
| **Total no fibres** | | 1721 ± 37 | | | 3811 ± 1079 | | | | 0.002 | |
| **Fibre diameter** | µm | 7.25 ± 0.39 | | | 3.37 ± 0.30 | | | | $<10^{-4}$ | |
| **Fibre diameter full range** | µm | 1.65 - 15.87 | | | 1.35 - 12.95 | | | | | |
| **Nerve area** | $\mu m^2$ | $1.78 \cdot 10^5 \pm 0.19$ | | | $1.68 \cdot 10^5 \pm 0.70$ | | | | 0.662 | |
| **Mean fibre area** | $\mu m^2$ | 47.93 ± 5.05 | | | 10.36 ± 2.02 | | | | $<10^{-4}$ | |
| **Mean fibre area full range** | µm | 2.13–197.77 | | | 1.53 - 131.77 | | | | | |
| **Fibre density (no/1000)** | $\mu m^{-2}$ | 9.77 ± 1.00 | | | 20.99 ± 5.83 | | | | 0.002 | |
| **Relative area of interspace** | % | 53.5 ± 2.0 | | | 77.8 ± 8.6 | | | | $<10^{-4}$ | |
| | | **α** | **β** | $\mathbf{p_{\alpha\beta}}$ | **α** | **β** | $\mathbf{p_{\alpha\beta}}$ | $\mathbf{p_{\alpha\alpha}}$ | $\mathbf{p_{\beta\beta}}$ | $\mathbf{p_{\alpha\beta 2}}$ |
| $\mathbf{F_{max,\alpha/\beta}}$ | % | 0.78 ± 0.15 | 1.1 ± 0.04 | 0.003 | 2.88 ± 0.61 | 1.69 ± 1.03 | 0.001 | $<10^{-4}$ | 0.141 | 0.054 |
| $\mathbf{d_{Fmax,\alpha/\beta}}$ | µm | 9.00 ± 0.22 | 4.36 ± 0.25 | $<10^{-4}$ | 2.97 ± 0.30 | 2.09 ± 0.05 | $<10^{-4}$ | $<10^{-4}$ | $<10^{-4}$ | $<10^{-4}$ |
| $\mathbf{w_{\alpha/\beta}}$ | | 0.23 ± 0.03 | 0.46 ± 0.05 | $<10^{-4}$ | 0.35 ± 0.04 | 0.23 ± 0.04 | $<10^{-4}$ | $<10^{-4}$ | $<10^{-4}$ | 0.5 |
| **Fibre number** | | 691 | 1030 | | 3023 | 792 | | | | |

The sum of the number of measured fibres in the samples which were used for the evaluations described is 2421 for the control nerves and 15560 for the regenerating nerves. Values are represented as mean ± SD. The significance of the differences between the values is represented as $p_{\alpha\beta}$, $p_{\alpha\alpha}$, $p_{\beta\beta}$, and $p_{\alpha\beta 2}$. The subscript indicates the fibre classes relevant to the comparison. Additionally, the values of the control nerve Aβ-fibre population were compared with the values of the regenerating nerve for the Aα-fibre population, and the significance of differences was represented as $p_{\alpha\beta 2}$. Vice versa comparison yielded significant differences for all parameters ($p<10^{-4}$).



values of $d_{Fmax,\alpha}$ and $d_{Fmax,\beta}$ were only slightly, though significantly, different. Consequently, the diameter distributions of both populations overlapped considerably.

In both control and regenerating nerves, the AIC was lower for fitting the sum of two com - pared to one lognormal function.

## Discussion

Twelve weeks after sciatic nerve autografting, the number of nerve fibres in the peroneal nerve was doubled, and the fibre diameter was halved. *In vitro* electrophysiology of the grafted sciatic nerve demonstrated that the mean conduction velocity decreased to one third, the mean firing threshold quadrupled, the mean refractory period doubled, and the total charge displaced during the compound action potential halved. Of these parameters only the number and diameter of the nerve fibres and the mean conduction velocity can be compared against previous results. There are no comparable data in literature for the other parameters.

The number of nerve fibres, the diameter most frequently present and its range in the peroneal nerves of control and autografted animals were similar to those reported by others

*Figure 5.* Frequency distributions of nerve fibre diameter of the peroneal nerve.

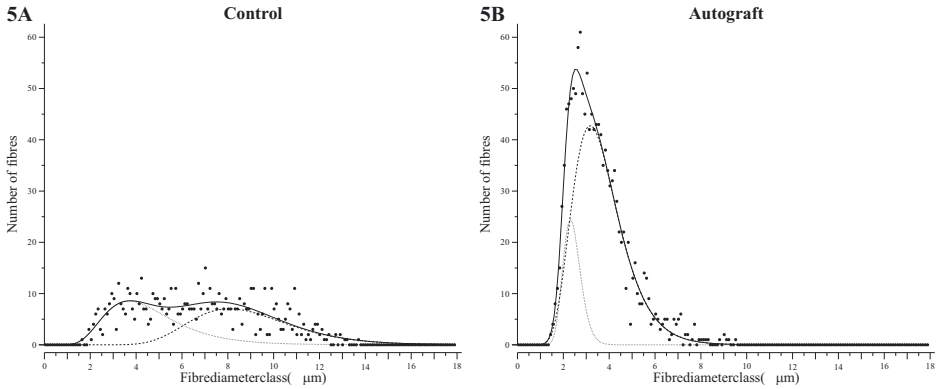


Typical examples of peroneal nerve fibre diameter frequency distributions from control (fig. 5A) and autografted (fig. 5B) rats. The data were obtained from the same control and autografted nerves as represented in figures 2 and 3. For each graph, the diameters of the nerve fibres were distributed into 180 classes of 0.1 µm each, and plotted against the number of fibres present in that class. The dots represent the number of fibres per diameter class, the solid line represents the fitted total curve, the dashed line the Aα-fibre population, and the dotted line the Aβ-fibre population.



[9, 18, 35, 36], though some reported that the number of fibres in autografted nerves did not change [12, 32].

In control nerves, we measured an MCV of 39 m/s *in vitro* at room temperature, comparable to the 30 m/s described by van den Berg [48]. In autografts, we measured an MCV of 12.5 m/s, representing a reduction to 30% of the control value. This reduction is in accordance to results reported by others [19, 34] (normal nerves) [11] (autografted nerves). The smaller fibre diameters and thinner myelin sheaths that we observed in regenerating nerves, as well as the decreased internodal distance [39], largely account for the decrease in MCV.

In order to relate the morphological data to the electrophysiological data, we will use the empirical inverse relations between extracellular firing threshold and diameter [cf. 6, 42] and refractory period and diameter [37]. The expected relation between $Q_{max}$ and the number of nerve fibres (N) and the fibre diameter (d) is given below. In normal nerves, the amplitude of the monophasic action current, is expected to be proportional to the square of the axon diameter [42]. Since the displaced charge is given by the product of the height of the action current and its duration, the dependence of duration on fibre diameter is important. Rushton's theory predicts that spike duration is independent of fibre diameter, but Paintal's data seem to show a weak inverse relation [cf. 38]. However, it was argued that such a relation could have artifactually resulted from the recording of a crushed nerve end [40]. Therefore we take the "constancy of the duration of the spikes of all fibres of the A group" as found by Gasser and Grundfest [23] for granted. Thus Q can be taken proportional to the square of the axon diameter, and consequently to the square of the fibre diameter [42]. Assuming that each fibre of a particular diameter contributes an equal amount of charge, the total charge by that fibre group would be proportional to the total number of fibres present (N). Taken together for a

particular fibre group we expect that the displaced charge is proportional to the product of N and $d^2$. Since only diameter and number are involved, this relation should also hold for the regenerating nerve. It should be noted, however, that the $Nd^2$-relation is valid only as long as other determiners of the electrophysiological properties of the regenerating nerve fibre, like its ion channel expression, remain unchanged.

### *Aα- and Aβ-fibres in control nerves*

In control nerves, two fibre populations were distinguished by fitting the sum of two *erf*-functions (eq. 2) to the stimulus-recruitment curves, and by fitting the sum of two lognormal functions (eq. 4) to the fibre diameter distribution curve. The presence of two peaks at 4 and 9 µm was in agreement with the peaks described by Chamberlain [8]. Since the range of the conduction velocities of our control nerves fell within the range of the faster myelinated nerve fibres, we designated these two populations as the Aα- and the Aβ-fibre-populations [33]. The $d_{Fmax,\alpha}$ and $d_{Fmax,\beta}$ differed by a factor two, in perfect agreement with the ratio of the firing thresholds of the two populations. The number of the Aβ-fibres was about 1.5 times the number of the Aα-fibres. Consequently the ratio of $Q_{max,\alpha}$ and $Q_{max,\beta}$ was proportional to $N_\alpha(d_{Fmax,\alpha})^2/N_\beta(d_{Fmax,\beta})^2$, as predicted.

Two fibre populations were also distinguished by fitting the sum of two *erf*-functions (eq. 3) to the interpulse time-recruitment curves. The identity of the two sets of fibre populations was confirmed by the equality of the second, independent estimates of $Q_{max,\alpha}$ and $Q_{max,\beta}$ to those derived from the stimulus recruitment curves. This equality strongly supports the validity of the model. The value of $t_{50,\beta}$ was twice the value of $t_{50,\alpha}$, in agreement with the ratio of the Aα- and the Aβ-fibre diameters.

The agreement of the values of $V_{50}$, $t_{50}$, and $Q_{max}$ with the predictions based on number of fibres and fibre diameters supports the view that the two populations envisioned electrophysiologically are identical to the populations distinguished morphometrically. Moreover, it signifies that the Aα- and Aβ-fibres differ only in diameter and number, and that their ion channel composition is equal.

### *Aα- and Aβ-fibres in autografted nerves*

The two populations that were distinguished in the autografted nerves differed by a factor two in mean threshold, and a factor three in mean refractory period. Since the range of the conduction velocities still conformed to the range of the faster myelinated nerve fibres, we designated these populations again as Aα- and Aβ-fibres. Two populations could also be distinguished morphometrically in agreement with literature [4, 24, 36]. The nerve fibres with the largest diameter were considered to represent the Aα-fibres, and those with the smallest diameter the Aβ-fibres. The values of $d_{Fmax,\alpha}$ and $d_{Fmax,\beta}$ were 3 and 2 µm, respectively. Neither the ratio of the firing thresholds of the Aα- and Aβ-fibres, nor their refractory periods are inversely proportional to the ratio of their fibre diameters in the autografted nerve.

The values of $Q_{max,\alpha}$ and $Q_{max,\beta}$ estimated from the stimulus recruitment data were equal, but $Q_{max,\beta}$ estimated from the interpulse time recruitment data was only half the corresponding value of $Q_{max,\alpha}$. As the separation of the Aα- and Aβ-fibre populations is larger in the interpulse time recruitment experiment (compare $t_{50,\beta}/t_{50,\alpha}$ and $V_{50,\beta}/V_{50,\alpha}$), and as the standard deviation of $Q_{max,\alpha}$ and $Q_{max,\beta}$ as estimated from the the interpulse time recruitment data is smaller, we consider the value of $Q_{max,\beta}$ derived from this experiment the most trustworthy. The increase in the number of nerve fibres was exclusively caused by a fourfold increase in the number of Aα-fibres, while the number of Aβ-fibres remained the same. Consequently the ratio of $Q_{max,\alpha}$ and $Q_{max,\beta}$ was never proportional to $N_{\alpha}(d_{Fmax,\alpha})^2/N_{\beta}(d_{Fmax,\beta})^2$, neither as estimated from the stimulus recruitment data, nor from the interpulse time-recruitment data. However, $V_{50}$, $t_{50}$, and $Q_{max}$ would only solely be dictated by number and diameter, if the electrical properties of the regenerating nerve fibres were unchanged.



*Comparison of Aα- and Aβ-fibres in control and autografted nerves*

The regenerating Aα-fibres demonstrated a threefold increase in $V_{50}$, in excellent agreement with the threefold decrease in their $d_{Fmax,\alpha}$. Furthermore, compared to the $Q_{max,\alpha}$ of the control nerves, the $Q_{max,\alpha}$ of autografted nerves is proportional to $N_{\alpha,control}(d_{Fmax,\alpha,control})^2/ N_{\alpha,grafted}(d_{Fmax,\alpha,grafted})^2$, as predicted. These facts support the presumption that this population indeed represents the Aα-fibres of the autografted nerve. The value of $t_{50,\alpha}$ in the autografted nerve, however, increased only with a factor 1.3, less than expected from the threefold decrease in their $d_{Fmax,\alpha}$. Upregulation of the $Na_{v1.3}$ channels as observed in spinal sensory neurons after axotomy [51], would shorten the refractory period [10]. A comparable upregulation in the regenerating Aα-fibres would cause $t_{50,\alpha}$ to increase less than predicted from their decreased diameter only. A study into cat ventral spinal root regeneration demonstrated, however, that the number of sodium channels per node remained normal or was only slightly increased sixteen to forty-five weeks after cryoaxotomy [39]. Concomitantly we expect that the expression of the $Na_{v1.3}$ channels in the Aα-fibres will eventually decrease, and in a separate study we indeed established that the $Na_{v1.3}$ channel expression is only temporarily upregulated in the sciatic nerve after crush lesions [52].

In the regenerating Aβ-fibres, to the contrary, $t_{50,\beta}$ did change proportional to the value of $d_{Fmax,\beta}$. The value of $t_{50,\beta}$ of the regenerating Aβ-fibres doubled, in agreement with the twofold decrease in their value of $d_{Fmax,\beta}$. The value of $V_{50,\beta}$ increased almost threefold, more than expected based on the twofold increase of the value of $d_{Fmax,\beta}$. The firing threshold of the Aβ-fibres may be significantly affected by adjustments in the types of sodium channel that are expressed at the Ranvier nodes of regenerated nerve fibres. For instance, a decrease in the number density of the sodium channel $Na_{v1.6}$, predominantly present in the nodal membrane of peripheral nerves [7], would be expected to increase the firing threshold. In the DRG neuron, such decreases have indeed been found for the sodium channel isoforms $Na_{v1.8}$ and $Na_{v1.9}$ [45] after transection of the rat sciatic nerve. A comparable downregulation of the $Na_{v1.6}$ channel may explain the fact that $V_{50,\beta}$ increased more than expected on basis of diameter only. In a

separate study we established that, after crush lesions of the sciatic nerve, not only the $Na_{v1.6}$ expression at the nodal membrane decreases, but moreover the expression of the potassium channel isoforms $K_{v1.1}$ and $K_{v1.2}$ increases at the nodal membrane [52]. Increased potassium channel expression at the nodal membrane will also contribute to the increase of the firing threshold. The value of $Q_{max,\beta}$ remained the same, in contrast to the fivefold lower value of $Q_{max,\beta}$ predicted by $N_{\beta,control}(d_{Fmax,\beta,control})^2/N_{\beta,grafted}(d_{Fmax,\beta,grafted})^2$. Repetitive firing of regenerating Aβ-fibres, as has been demonstrated to occur after applying single pulse stimuli, probably arises from adjustments in the ratio of sodium and potassium channels [2]. Repetitive firing may have increased the measured value of $Q_{max,\beta}$.

In summary, mathematical functions were fitted to electrophysiological and morphometrical datasets of normal and autografted nerves, and parameters were derived (charge displaced, fibre number, fibre diameter, firing threshold, refractory period) that described subpopulations of the nerve fibres present in the sciatic nerve. Given the remarkable consistency of the control nerve parameters with predictions based on simple geometrical and numerical considerations, we concluded that these subpopulations could only be the Aα- and Aβ-fibre populations. Surprisingly, the increase of the number of nerve fibres present twelve weeks after autografting was exclusively caused by an increase of the Aα-fibres, indicating that at least the Aα-fibres branch extensively. In regenerating nerves $Q_{max,\alpha}$, $V_{50,\alpha}$ and $t_{50,\beta}$ changed proportional to changes of their respective fibre number and diameter. In contrast, the values of $Q_{max,\beta}$, $V_{50,\beta}$ and $t_{50,\alpha}$ in the regenerating nerve were different from the predicted values.

Thus, *in vitro* electrophysiological evaluation of the sciatic nerve yields parameters that discriminate normal from autografted nerves. These parameters alone will be useful to estimate the quality of regeneration in, for instance, synthetic nerve conduits. However, the application of mathematical models to the electrophysiological data furthermore allows to estimate the values of these same parameters for the Aα- and Aβ-fibre populations. Based on established empirical relations, these data can be correlated with similarly analyzed morphometrical data, enabling deduction of specific changes that have occurred in the regenerating Aα- and Aβ-fibres. This demonstrates that the combination of electrophysiological and morphometrical evaluation methods yields a more profound insight into the quality of regeneration than morphometrical analysis alone.



## Acknowledgements

We wish to thank Dr. S. LeCessie and Dr. P. Eilers for help with the statistical analysis of the data, A. Abrahams-Sutton for correction of the manuscript, and H. Choufoer for technical assistance.

## References


1. Abramowitz, M., and Stegun, I. A. 1965. Handbook of mathematical functions, U.S. National Bureau of Standards (1964). Dover, New York.
2. Amir, R., Michaelis, M., and Devor, M., 2002. Burst discharge in primary sensory neurons: triggered by subthreshold oscillations, maintained by depolarizing afterpotentials. J. Neurosci. 22, 1187-1198.
3. Ansselin, A. D., Fink, T., and Davey, D. F., 1997. Peripheral nerve regeneration through nerve guides seeded with adult Schwann cells. Neuropathol. Appl. Neurobiol. 23, 387-398.
4. Archibald, S. J., Shefner, J., Krarup, C., and Madison, R. D., 1995. Monkey median nerve repaired by nerve graft or collagen nerve guide tube. J. Neurosci. 15, 4109-4123.
5. Bertelli, J. A., Mira, J. C., Pecot-Dechavassine, M., and Sebille, A., 1997. Selective motor hyperrein - nervation using motor rootlet transfer: an experimental study in rat brachial plexus. J. Neurosurg. 87, 79-84.
6. Blair, E. A., and Erlanger, J., 1933. A comparison of the characteristics of axons through their indi - vidual electrical responses. Am. J. Physiol. 106, 524-564.
7. Caldwell, J. H., Schaller, K. L., Lasher, R. S., Peles, E., and Levinson, S. R., 2000. Sodium channel Na(v)1.6 is localized at nodes of Ranvier, dendrites, and synapses. Proc. Natl. Acad. Sci. U S A 97, 5616-5620.
8. Chamberlain, L. J., Yannas, I. V., Hsu, H. P., Strichartz, G., and Spector, M., 1998. Collagen-GAG sub - strate enhances the quality of nerve regeneration through collagen tubes up to level of autograft. Exp. Neurol. 15, 315-329.
9. Chamberlain, L. J., Yannas, I. V., Hsu, H. P., Strichartz, G. R., and Spector, M., 2000. Near-terminus axonal structure and function following rat sciatic nerve regeneration through a collagen-GAG matrix in a ten-millimeter gap. J. Neurosci. Res. 60, 666-677.
10. Cummins, T. R., and Waxman, S. G., 1997. Downregulation of tetrodotoxin-resistant sodium cur - rents and upregulation of a rapidly repriming tetrodotoxin-sensitive sodium current in small spinal sensory neurons after nerve injury. J. Neurosci. 17, 3503-3514.
11. Dubuisson, A. S., Foidart-Dessalle, M., Reznik, M., Grosdent, J. C., and Stevenaert, A., 1997. Prede - generated nerve allografts versus fresh nerve allografts in nerve repair. Exp. Neurol. 148, 378-387.
12. Evans, P. J., MacKinnon, S. E., Midha, R., Wade, J. A., Hunter, D. A., Nakao, Y., and Hare, G. M., 1999. Regeneration across cold preserved peripheral nerve allografts. Microsurgery 19, 115-127.
13. Feirabend, H. K. P. 1983. Anatomy and development of longitudinal patterns in the architecture of the cerebellum of the white leghorn (Gallus domesticus). Thesis, University of Leiden, Leiden, the Netherlands.
14. Feirabend, H. K. P., Choufoer, H., and Ploeger, S., 1998. Preservation and staining of myelinated nerve fibers. Methods 15, 123-131.
15. Feirabend, H. K. P., Choufoer, H., and Voogd, J., 1996. White matter of the cerebellum of the chicken (Gallus domesticus): a quantitative light and electron microscopic analysis of myelinated fibers and fiber compartments. J. Comp. Neurol. 369, 236-251.
16. Feirabend, H. K. P., Kok, P., Choufoer, H., and Ploeger, S., 1994. Preservation of myelinated fibers for electron microscopy: a qualitative comparison of aldehyde fixation, microwave stabilisation and other procedures all completed by osmication. J. Neurosci. Meth. 55, 137-153.
17. Fields, R. D., and Ellisman, M. H., 1986a. Axons regenerated through silicone tube splices. I. Con - duction properties. Exp. Neurol. 92, 48-60.
18. Fields, R. D., and Ellisman, M. H., 1986b. Axons regenerated through silicone tube splices. II. Func - tional morphology. Exp. Neurol. 92, 61-74.

19. Foidart-Dessalle, M., Dubuisson, A., Lejeune, A., Severyns, A., Manassis, Y., Delree, P., Crielaard, J. M., Bassleer, R., and Lejeune, G., 1997. Sciatic nerve regeneration through venous or nervous grafts in the rat. Exp. Neurol. 148, 236-246.
20. Francel, P. C., Francel, T. J., MacKinnon, S. E., and Hertl, C., 1997. Enhancing nerve regeneration across a silicone tube conduit by using interposed short-segment nerve grafts. J. Neurosurg. 87, 887-892.
21. Francel, P. C., Smith, K. S., Stevens, F. A., Kim, S. C., Gossett, J., Gossett, C., Davis, M. E., Lenaerts, M., and Tompkins, P., 2003. Regeneration of rat sciatic nerve across a LactoSorb bioresorbable conduit with interposed short-segment nerve grafts. J. Neurosurg. 99, 549-554.
22. Fugleholm, K., Schmalbruch, H., and Krarup, C., 1994. Early peripheral nerve regeneration after crushing, sectioning, and freeze studied by implanted electrodes in the cat. J. Neurosci. 14, 2659-2673.
23. Gasser, H. S., and Grundfest, H., 1939. Axon diameters in relation to the spike dimensions and the conduction velocity in mammalian A fibers. Am. J. Physiol. 127, 393-414.
24. Gutmann, E., and Sanders, F. K., 1943. Recovery of fibre numbers and diameters in the regeneration of peripheral nerves. J. Physiol. 101, 489-518.
25. Jack, J. J. B., Noble, D., and Tsien, R. W. 1983. Electric current flow in excitable cells. Oxford University Press.
26. Jenq, C. B., and Coggeshall, R. E., 1985. Numbers of regenerating axons in parent and tributary peripheral nerves in the rat. Brain Res. 326, 27-40.
27. Kakinoki, R., Nishijima, N., Ueba, Y., Oka, M., Yamamuro, T., and Nakamura, T., 1998. Nerve regeneration over a 20-mm gap through a nerve conduit containing blood vessels in rats: the influence of interstump distance on nerve regeneration. J. Neurosurg. Sci. 42, 11-21.
28. Keeley, R., Atagi, T., Sabelman, E., Padilla, J., Kadlcik, S., Keeley, A., Nguyen, K., and Rosen, J., 1993. Peripheral nerve regeneration across 14-mm gaps: a comparison of autograft and entubulation repair methods in the rat. J. Reconstr. Microsurg. 9, 349-358.
29. Kimura, J., 1981. Refractory period measurement in the clinical domain. Adv. Neurol. 31, 239-265.
30. Kolmogorov, A., 1941. Confidence limits for an unknown distribution function. Ann. Meth. Statist. 12, 461-463.
31. Krarup, C., Horowitz, S. H., and Dahl, K., 1992. The influence of the stimulus on normal sural nerve conduction velocity: a study of the latency of activation. Muscle Nerve 15, 813-821.
32. Le Beau, J. M., Ellisman, M. H., and Powell, H. C., 1988. Ultrastructural and morphometric analysis of long-term peripheral nerve regeneration through silicone tubes. J. Neurocytol. 17, 161-172.
33. Liu, C. N., Wall, P. D., Ben-Dor, E., Michaelis, M., Amir, R., and Devor, M., 2000. Tactile allodynia in the absence of C-fiber activation: altered firing properties of DRG neurons following spinal nerve injury. Pain 85, 503-521.
34. Maeda, T., MacKinnon, S. E., Best, T. J., Evans, P. J., Hunter, D. A., and Midha, R. T., 1993. Regeneration across 'stepping-stone' nerve grafts. Brain Res. 618, 196-202.
35. Meek, M. F., Robinson, P. H., Stokroos, I., Blaauw, E. H., Kors, G., and den Dunnen, W. F., 2001. Electron microscopical evaluation of short-term nerve regeneration through a thin-walled biodegradable poly(DLLA-epsilon-CL) nerve guide filled with modified denatured muscle tissue. Biomaterials 22, 1177-1185.
36. Mira, J. C., 1979. Quantitative studies of the regeneration of rat myelinated nerve fibres: variations in the number and size of regenerating fibres after repeated localized freezings. J. Anat. 129, 77-93.
37. Paintal, A. S., 1966. The influence of diameter of medullated nerve fibres of cats on the rising and falling phases of the spike and its recovery. J. Physiol. 184, 791-811.

38. Paintal, A. S., 1973. Conduction in mammalian nerve fibres, in New developments in electromyography and clinical neurophysiology, volume 2, Karger, Basel.
39. Querfurth, H.W., Armstrong, R., and Herndon, R.M., 1987. Sodium channels in normal and regenerated feline ventral spinal roots. J. Neurosci. 7, 1705-1716.
40. Ritchie, J. M., 1982. On the relation between fibre diameter and conduction velocity in myelinated nerve fibres. Proc. R. Soc. Lond. Biol. Sci. 217, 29-35.
41. Rosen, J. M., Padilla, J. A., Nguyen, K. D., Siedman, J., and Pha, H. N., 1992. Artificial nerve graft using glycolide trimethylene carbonate as a nerve conduit filled with collagen compared to sutured autograft in a rat model. J. Rehab. Res. 29, 1-12.
42. Rushton, W. A. H., 1951. A theory of the effects of fiber size in medullated nerve. J. Physiol. 115, 101-122.
43. Schmalbruch, H., 1986. Fiber composition of the rat sciatic nerve. Anat. Rec. 215, 71-81.
44. Seckel, B. R., Chiu, T. H., Nyilas, E., and Sidman, R. L., 1984. Nerve regeneration through synthetic biodegradable nerve guides: regulation by the target organ. Plast. Reconstr. Surg. 74, 173-181.
45. Sleeper, A. A., Cummins, T. R., Dib-Hajj, S. D., Hormuzdiar, W., Tyrrell, L., Waxman, S. G., and Black, J. A., 2000. Changes in expression of two tetrodotoxin-resistant sodium channels and their currents in dorsal root ganglion neurons after sciatic nerve injury but not rhizotomy. J. Neurosci. 20, 7279-7289.
46. Smirnow, N. V., 1948. Table for estimating the goodness of fit of empirical distributions. Ann. Meth. Statist. 19, 279-281.
47. Smith, K. J., 1978. A method to represent the spectrum of refractory periods of transmission of the constituent fibres of a nerve. J. Physiol. 278, 7P-9P.
48. Van den Berg, R. J., Versluys, C. A., de Vos, A., and Voskuyl, R. A., 1994. Nerve fiber size-related block of action currents by phenytoin in mammalian nerve. Epilepsia 35, 1279-1288.
49. Veltink, P. H., Van Alste, J. A., and Boom, H. B., 1988. Influences of stimulation conditions on recruitment of myelinated nerve fibers: a model study. IEEE Trans. Biomed. Eng. 35, 917-924.
50. Wang, S., Wan, A. C., Xu, X., Gao, S., Mao, H. Q., Leong, K. W., and Yu, H., 2001. A new nerve guide conduit material composed of a biodegradable poly(phosphoester). Biomaterials 22, 1157-1169.
51. Waxman, S. G., 2001. Transcriptional channelopathies: an emerging class of disorders. Nat. Rev. Neurosci. 2, 652-659.
52. Wolfs, J. F. C., Vleggeert-Lankamp, C. L. A. M., Lakke, E. A. J. F., and Thomeer, R. T. W. M., 2003. Ion channel redistribution over time in crushed rat sciatic nerve. Program No 41.4. Abstract Viewer/Itinerary Planner. Washington, DC: Society for Neuroscience.
53. Yoshii, S., Oka, M., Ikeda, N., Akagi, M., Matsusue, Y., and Nakamura, T., 2001. Bridging a peripheral nerve defect using collagen filaments. J. Hand. Surg. [Am.] 26, 52-59.